Theoretical investigation on the geometries of DOTA and DOTA-like complexes and on the transition states of their conformational equilibria†

Massimo Di Vaira* and Piero Stoppioni

Dipartimento di Chimica, Università di Firenze, via Maragliano, 77, 50144 Firenze, Italy. E-mail: massimo.divaira@unifi.it

Received (in Montpellier, France) 11th July 2001, Accepted 8th October 2001
First published as an Advance Article on the web 8th January 2002

Computations, mostly at the RHF level, have been performed on La^{3+} and Y^{3+} model complexes of the widely used DOTA ligand [DOTA = 1,4,7,10-tetraaza-1,4,7,10-tetrakis(carboxymethyl)cyclododecane] for the purpose of identifying properties of the transition states of geometrical isomer interconversions, which have been the object of numerous NMR studies. An analogous study has been carried out on model complexes of the same trications formed by the DOTA-like ligand 1,7-bis(1-methylimidazol-2-ylmethyl)-4,10-bis(carboxymethyl)-1,4,7,10-tetraazacyclododecane, LH_2. Features of the transition states for the two types of systems are compared.

In the last decades much interest has developed in the coordination chemistry of the functionalized macrocycle DOTA [1,4,7,10-tetraaza-1,4,7,10-tetrakis(carboxymethyl)-cyclododecane] and related ligands, both from the experimental[1–12] and the theoretical[13–19] point of view. Lanthanide DOTA complexes, in particular, due to their stability and to their paramagnetic properties, are candidates for use as contrast agents in the magnetic resonance imaging technique and the gadolinium complex is actually used to such purpose. Early NMR studies on the solution structures and dynamics of the lanthanide DOTA complexes pointed to the existence of two accessible conformers,[3] which was later confirmed by X-ray structural investigations.[4–9] These geometrical isomers, traditionally denoted M and m (or M_1, M_2 and m_1, m_2 when their enantiomeric pairs are considered[11]) present the metal atom eight-coordinated by the four nitrogen atoms of the macrocycle and by four carboxylic oxygens. The two sets of donor atoms are arranged in a quasi-antiprismatic geometry (M) about the metal atom or according to an "inverted antiprismatic" geometry (m), closer than the former to that of a regular prism.[3,11] For clarity these geometries, as provided by two of the present calculations, are schematically shown in Fig. 1, with the conventional notation.[11,20] It should be noted that inversion of chirality of one of the ring systems, either macrocylic or carboxylic, is sufficient to switch between the M and m geometry types (this is rationalized by considering both enantiomer pairs of the M as well as of the m conformer), at least as far as the overall chirality properties are concerned, ignoring the small amount of overall relaxation that is involved.

Recently, a DOTA-like ligand based on the 1,4,7,10-tetraazacyclododecane macrocycle with mixed carboxylic and methylimidazolic functions [1,7-bis(1-methylimidazol-2-ylmethyl)-4,10-bis(carboxymethyl)-1,4,7,10-tetraazacyclododecane, LH_2] has been synthesized in this laboratory and the structures of its zinc and nickel complexes, with the ligand in partially or totally deprotonated form, have been investigated.[21] Lanthanide complexes of the deprotonated ligand, L^{2-}, have also been obtained and their NMR spectra have been rationalized[22] on similar grounds to those of the DOTA compounds, based on the key assumption of the existence of two conformers in solution.[3]

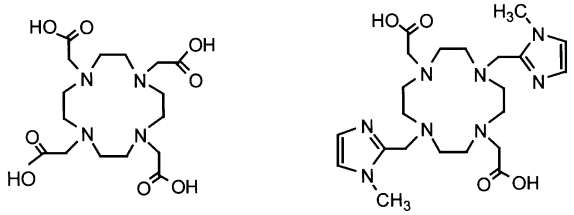

It is of interest to obtain information on the energetic and structural aspects of the interconversion processes between isomers of complexes of these types. Since detachment of the pendant arms in the course of such processes is excluded on the basis of the NMR spectra,[3,12,22] the interconversions between the four stereoisomers may be expected to occur *via* either stepwise or synchronous changes in the chirality of the pendant arms and/or of the macrocycle ethylenic chains.[12] In the present work, the energies of stereoisomers of DOTA and of DOTA-like L^{2-} complexes formed by metal trications and the possible pathways for their interconversions have been investigated by quantum mechanical procedures on model systems in the gaseous state. A comparatively larger effort was dedicated to the study of the DOTA models, which are relatively less demanding than the L^{2-} ones from the computational point of view. The models were generally, although not always, simplified by omitting the coligand water molecule lying in the capping position, opposite the macrocycle, which has been detected in the majority of the solid state structures[4–7] and is assumed to be present in solution for most of these systems, based on exhaustive experimental evidence.[12] However, the conclusions drawn here, mostly based on intersystem comparisons, should not be too adversely affected by such an omission, in view of the conceivable weakness of the

† Electronic supplementary information (ESI) available: Tables S1–S3, extended versions of Tables 1–3, and Table S4, comparison of structural features. See http://www.rsc.org/suppdata/nj/b1/b106168m/

 DOI: 10.1039/b106168m

This journal is © The Royal Society of Chemistry and the Centre National de la Recherche Scientifique 2002

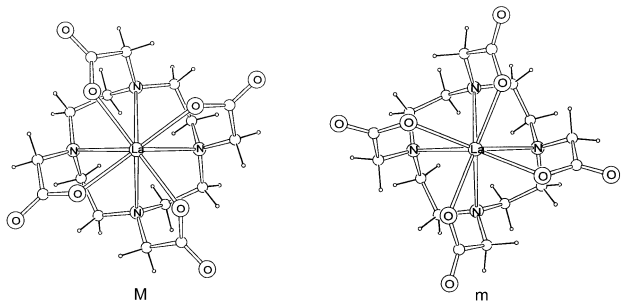

Fig. 1 The two fundamental geometries, referred to as M and m in the literature on DOTA complexes, may be identified through the signs, and associated symbols, of the torsion angles formed by the macrocycle ring chains (positive sign, right-handed helicity, δ symbol; negative, left-handed, λ) and those of the pendant arms (Δ or Λ for overall positive/negative torsion angles or right/left-handed helicity of the arms).[11,20] In this notation the M isomer in the figure is Δ(λλλλ), corresponding in particular to the M_1 isomer of ref. 11 [the M_2 enantiomer has chirality Λ(δδδδ)] and the m isomer shown corresponds to m_1 [Λ(λλλλ)] of ref. 11, the m_2 enantiomer being Δ(δδδδ).

interaction between the metal cation and the water oxygen, compared to those with the charged oxygen donor atoms of the macrocyclic ligand. In spite of the limitations imposed by the complexity of the calculations some trends have emerged. The purpose of this work is to attempt to shed some light on properties of these systems not directly obtainable from experiment, possibly with a view to more accurate calculations in the future.

Computational details

Preliminary calculations were performed with molecular mechanics procedures, with the parameters available for the MMX force field of PCMODEL 7.0[23] and for the MM+ force field of Hyperchem 5.0.[24] Hyperchem's semiempirical ZINDO/1 program was also employed. All final calculations, whose results are reported here, were performed using the Gaussian 98 suite of programs,[25] by the RHF or, to a lesser extent, the B3LYP[26,27] method with a variety of basis sets. Results are reported for calculations generally employing the effective core potential (ECP) and valence LanL2DZ functions[28] for the La and Y metal atoms and the 6-31G basis[29] for the H, C, N and O atoms. This combination will be referred to as basis set A. The non-metal atom basis 6-311G(d,p)[30,31] supplemented with diffuse functions for the oxygens, was used in some of the calculations (basis set B, including the LanL2DZ metal functions). The SDD[32,33] effective core and valence functions of Gaussian 98 were used for the Lu atom and, in a few comparison calculations, also for La and Y; their combination with the 6-31G basis for non-metal atoms will be referred to as A′ basis set. Due to the relative complexity of the systems full characterization of their geometries through frequency calculations was performed only in a limited number of cases, for example, for the main, water-free, $LaDOTA^-$ models optimized at the RHF/A level. In view of the similarity of structural types it may be confidently assumed that the optimized Y and Lu models also correspond to true energy minima. On the other hand, the transition state geometries were consistently characterized by the search algorithm[34] as being associated with one imaginary vibrational frequency. For the analysis of geometrical results and for graphics PARST,[35] Molden[36] and OrtepIII[37] were employed. The computations were performed on PCs running under Linux, implemented by Prof. Alessandro Bencini of our department.

Results and discussion

Geometries of DOTA models

As mentioned in the Introduction, the lanthanide DOTA complexes (these are monoanionic species due to full deprotonation of the ligand) generally bear a capping water molecule in solution, so that the metal ion is nine-coordinated, although the monodentate ligand is much more labile than the polydentate one. Excluding for practical reasons the water molecule from the model for most of the calculations may have affected to a limited extent the optimized geometries (see below), but it should not have adversely affected the general conclusions about the nature of the transition states, which are apparently controlled by the stronger interactions due to the polydentate ligand. The optimizations of models including the water coligand were lengthy and difficult, evidently due to the complexity of the potential energy surfaces. Depending on details of the starting geometries, as well as on the specific computational procedures used (*e.g.*, DFT-B3LYP *vs.* RHF), both $LaDOTA(H_2O)^-$ optimized geometries with a "vertically" oriented water molecule, and geometries with a "bent" water molecule, engaged in hydrogen bonds with DOTA oxygens, were identified. Two of these are shown in Fig. 2.‡ On the other hand, the $YDOTA(H_2O)^-$ models, irrespective of isomer type and of starting conditions, optimized in all cases to geometries with a bent, hydrogen bonded water molecule, probably as a consequence of easier hydrogen bond formation than in the La systems, due to the shorter $Y–O_w$ distance than the $La–O_w$ one. In view of the complexity of the optimization procedures and of the variety of results, it was apparent that inclusion of the water coligand in the search for transition state geometries by the present approaches would have presented prohibitive difficulties. In most of the calculations the closed shell La^{3+} and Y^{3+} metal ions were considered, to trace metal size effects between conditions approximately existing at the extremes of the lanthanide series. Systems with the Lu^{3+} cation were studied for limited comparison purposes and results are reported in the ESI.

Essential geometrical data and energy differences between models from this first set of calculations are reported in Tables 1 and S1 according to the criteria specified in the footnote. The following points, emerging from inspection of the data in Table 1, deserve comment, also for the purpose of evaluating the reliability and limitations of the procedures. The metal–donor atom distances for the water-free systems formed by the different cations substantially bracket those from the previous theoretical study on Gd^{3+} complexes[16] and roughly agree with experimental values [La–N 2.78(2) Å and La–O 2.50(2) Å,[8] Y–N 2.64(2) Å and Y–O 2.32(1) Å,[5,6] each being the mean of eight values obtained from the $LaDOTA^-$ and LaHDOTA moieties of a single structure, interlinked *via* capping carboxylate oxygens,[8] and from two monomeric $YDOTA(H_2O)^-$ complexes[5,6]].

‡ With reference to the notation in Fig. 2(a), the geometrical parameters whose values are reported in the tables are metal–nitrogen distances (D_N), metal–oxygen distances (D_O), N–C–C–O pendant arm torsion angles (T_{NO}), N–C–C–N macrocycle chelate ring torsion angles (T_{NN}). In C_4 symmetry only one value of each parameter is required. In lower symmetries a set of values (up to four) must be specified for each parameter. These are ordered in the tables according to the following convention: the first D_N value (leftmost of upper row in D_N four entries group) refers to an arbitrarily chosen macrocycle nitrogen [*e.g.*, N_1 in Fig. 2(a)], the first D_O value refers to the oxygen of that nitrogen's pendant arm (as shown in the figure), the first T_{NO} applies to the arm linking the above donor atoms and the first T_{NN} value is for the N–C–C–N chain formed by the above nitrogen (N_1) and the one (N_2) that follows in clockwise direction along the macrocycle, looking from the side of the carboxyl groups, as in Fig. 1 and 2(a). Similarly for the second value of each set (second D_N value pertaining to N_2, *etc.*) and so on, proceeding clockwise along the macrocycle and, in parallel, through the four entries of each group in the Table.

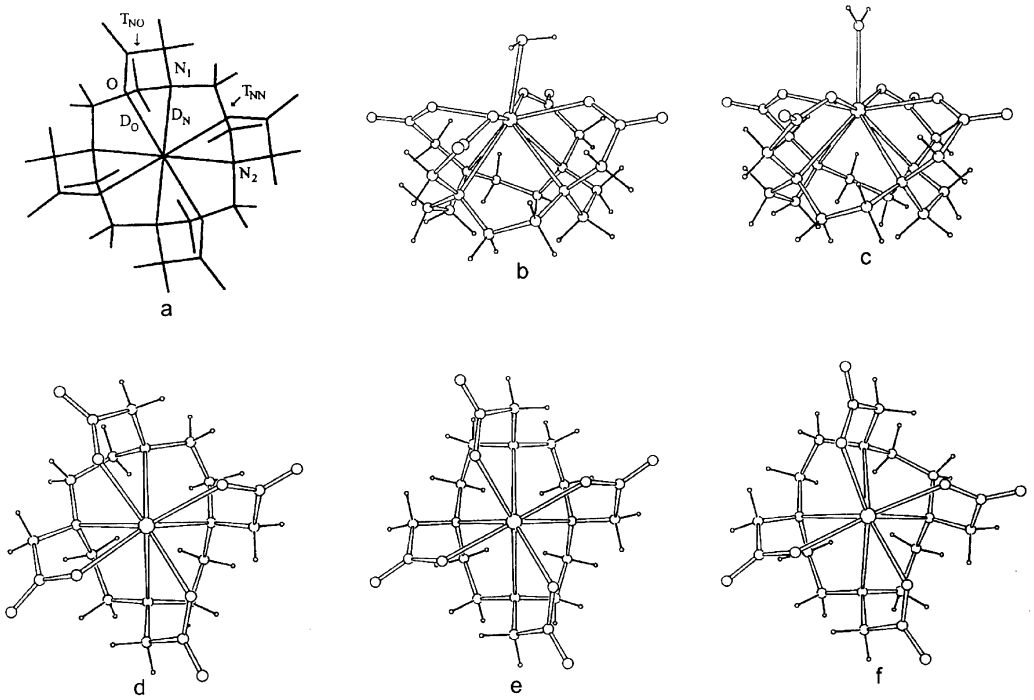

Fig. 2 (a) Sketch of the optimized LaDOTA$^-$ M_1 isomer exemplifying the notation used in the Tables (see footnote ‡ for conventions). (b) The M-type LaDOTA(H_2O)$^-$ complex optimized with H_2O in "bent" orientation. (c) M-type LaDOTA(H_2O)$^-$ with the alternative "vertical" H_2O arrangement. (d) Representation of the LaDOTA$^-$ p isomer (see Table 1). (e) LaDOTA$^-$ n isomer. (f) LaDOTA$^-$ q isomer.

However, the ratios between the values of the metal–oxygen and the metal–nitrogen distances for the individual models (D_O/D_N ratios, in the notation of Table 1) are smaller than expected. A similar effect has already been noted[16] and has been attributed to the use of effective core potentials (ECPs). The situation was only slightly improved by the use of the larger basis set B, intead of A (Table 1). Apart from the limited effect on the D_O/D_N values, the use of basis B, due to a better way of accounting for the donor atom lone pairs, produced some geometrical changes, particularly in the T_{NO} values (Table 1). However, the considerable increase in computational effort prevented a generalized use of that basis. Also the recourse to DFT calculations (results not reported) had only marginal effects on the metal–donor atom distances, in agreement with what was already observed for these substantially ionic metal–donor interactions, which do not involve large electronic correlation effects.[16] The inclusion of the coordinating water molecule produced either a small lengthening of *all* the metal–donor atom distances,

Table 1 Optimized geometries and energies of DOTA complexes formed by metal trications[a]

System	Basis set[b]	Geometry type[c]	D_N[d]	D_O[d] (D_{La-Ow})	T_{NO}[d]	T_{NN}[d]	ΔE[e] (E)
LaDOTA$^-$		M	2.880	2.441	41.3	−61.5	0 −1467.11752
		m	2.907	2.441	−34.4	−62.0	1.9
	A	p	2.953, 2.865 2.928, 2.850	2.448, 2.431 2.427, 2.449	46.0, 33.2 43.7, 39.7	58.7, −61.0 −53.8, −60.8	6.2
		n	2.863, 2.918	2.420, 2.459	36.5, 43.6	−53.9, 58.6	8.4
		q	3.074, 2.865 2.926, 2.827	2.433, 2.429 2.426, 2.461	43.4, 33.8 39.9, 30.6	57.8, 59.2 −60.1, 59.3	7.5
	B	M	2.883	2.463	38.1	−60.1	0 −1468.13960
		m	2.917	2.461	−32.4	−60.1	0.0
LaDOTA(H_2O)$^-$	A′	M[f]	2.90–2.94[g]	2.44–2.50 2.651[h]	41.0–43.7	−61.3 to − 62.5	0 −1543.46499
		m[f]	2.94–2.97	2.44–2.50 2.637[h]	−31.1 to − 35.5	−61.9 to − 62.7	2.4
		M[i]	2.91–2.92	2.46–2.47 2.565[h]	39.4–42.3	−61.0 to − 62.5	3.0
		m[i]	2.93–2.96	2.46–2.48 2.553[h]	−30.9 to − 32.6	−62.1 to − 62.3	4.8

[a] All results from RHF calculations. [b] The composition of the A, B and A′ basis sets is given in the text. [c] Geometries of the M and m type (isomers M_1 and m_1), both possessing C_4 symmetry in the absence of coordinating water molecule, are shown in Fig. 1 and those of type n (C_2 symmetry), p and q (both C_1) are shown in Fig. 2. Conformers n, p and q belong to an interconversion pathway between the M and m forms (see text). [d] Values of geometrical parameters [D_N and D_O distances (Å), T_{NO} and T_{NN} torsion angles (°)] are reported according to the criteria specified in footnote ‡ in the text. [e] Energy differences (ΔE) are in kcal mol^{-1} and the energy (E) of the reference model within each homogeneous group is given in Hartrees. [f] Model with "bent" water molecule, engaged in hydrogen bonds. [g] Ranges of values are given for the pseudo-C_4 models with H_2O (details in Table S1). [h] D_{La-Ow} value, metal–oxygen distance formed by H_2O. [i] Model with "vertical" H_2O.

leaving the mean value of the D_O/D_N ratio almost unchanged (La models, Table S1; the D_O distances formed by atoms involved in hydrogen bonding to the water molecule are in all cases appreciably longer than the other distances of the same type), or yielded a decrease in values of the ratio (Y models). Overall, as far as the metal–donor atom linkages are concerned, it would indeed appear[16] that the use of ECPs has the effect of accounting in a slightly different way for interactions possessing different amounts of ionic character.

The values of the macrocycle chains torsion angles (T_{NN} in Table 1) agree, within 1–2°, with the experimental ones, whereas the T_{NO} values differ significantly from the experimental ones, which range over 13–27° for the La structure,[8] and over 11–30°[5] and 12–32°[6] for the Y structures. The T_{NO} values for the M isomers in Table 1 compare more favourably with the 30.6° mean value of the arms torsion angles found for a dysprosium complex formed by the dtma ligand, closely related to DOTA.[12] Certainly, in the solid state structures the arrangement of the arms is subject to the effects of packing forces and to those of numerous hydrogen bonds; on the other hand, the computed T_{NO} values may be adversely affected more than other parameters by limitations of the basis set, in particular by the same factors that cause the above deviations in the D_O/D_N ratios from the experimental values. As far as the $LuDOTA^-$ models are concerned, their geometries (see ESI) are closely similar to those of the Y models, and similar considerations to those made above apply to the comparison with an experimentally determined structure.[7] The differences in bond distances to the metal between the Lu and Y models are substantially consistent with the difference in metal ionic radii.[38]

Further insight into the geometries and their variations is provided by consideration of the following geometrical parameters: the distances of the metal cation from the plane through the nitrogens (d_N) and from that through the coordinating oxygen atoms (d_O), the N···N distances between contiguous macrocycle nitrogens, the O···O distances between contiguous coordinating oxygens, and the N···O distances between donor atoms belonging to the same pendant arm. The last three parameters provide an estimate of the dimensions of the coordination cage and all of these values (Table S4) allow the effects of inclusion of the water molecule in the models to be monitored. On going from the M to the m isomer (water-free models), irrespective of the nature of the metal atom and in apparent contradiction to the trends in D_N and D_O values, *both* the d_N and the d_O value increase (by 0.06–0.08 Å), due to the rearrangement of the arms, even though the cage dimensions slightly decrease (N···N and O···O reductions $\leqslant$ 1%, N···O reduction $\leqslant$ 4%). On the other hand, as the metal atom varies from La to Y a decrease in d_N is found (0.18 Å, irrespective of the isomer), but an *increase* in d_O (0.13 Å for the M isomer, 0.10 Å for m). The latter increase is reconciled with the sensible reduction in D_O values (from La to Y models, Tables 1 and S1), considering that the O···O distances decrease considerably, by 9%, with decreasing size of the metal cation; the N···N and N···O distances, on the other hand, decrease much less ($\leqslant$ 2%). In a sense, the polydentate ligand wraps more tightly the metal cation of smaller size, reducing the span of its arms, while the cation shifts toward the macrocycle. Most of these trends are essentially preserved upon inclusion of the water coligand, with the possible exception of the trend in d_O values, which become less sensitive to changes in the nature of the metal atom. This is also found experimentally, although the experimental d_O values, reported in Table S4, are larger than the computed ones. The O···O separations increase by 2% (La) or 3% (Y) upon water inclusion, reaching values in good agreement with experiment.

In addition to the data for the two fundamental M and m geometries, data for three additional $LaDOTA^-$ minimum energy conformations are also reported in Table 1, where they are denoted as "n", "p" and "q". These, in particular the most symmetrical of them (n), were initially considered as conformers to be possibly taken into account for the rationalization of the NMR spectra. However, their energy separations from the most stable isomer, about three-four times as large as that between the m and M type models, seem to exclude their involvement as stationary states with significant weight in the thermal equilibria. On the other hand, these conformers were found to belong to a possible interconversion pathway between the main isomers, to be described below. For this reason, they are shown in Fig. 2. Strong similarities exist between the conformations attained by the macrocycle in the above energy minima and some of those predicted for cyclododecane.[39,40] The conformation in n corresponds to cyclododecane's [2424] form, according to Dale's nomenclature.[39] The mean of absolute differences between "corresponding" dihedral angles of the two rings (this quantity will be denoted "$|\Delta|$" hereafter, with reference to Anet and Rawdah's data[40]) amounts to 4.8°. For the [2334] arrangement of the macrocycle in both p and q, $|\Delta|$ is 7.6 and 8.7°, respectively. It has been pointed out[7] that the macrocycle in M and m adopts the [3333] conformation. More similarities of this type, also involving transition state geometries of the DOTA complexes as well as geometries of the DOTA-like ones, have been detected in this study and are reported in the following. All this suggests that geometric requirements of the twelve-membered ring tend to dominate not only the (directionally not very demanding) metal–donor atom interactions, but also the additional constraints posed by the presence of dangling groups in the ligand(s).

Energies of DOTA models

Turning to the energy values provided by the calculations, the M isomer is predicted to be more stable than the m one throughout ($E/\Delta E$ column in Table 1, A basis results), at variance with experiment, which indicates the m isomer to be of lower energy for large metal cations like La^{3+} (in nine-coordinate complexes, containing the water coligand).[11] It should be noted that the computed energy gap between the m and M lanthanum models, not large, reduces to 1.2 kcal mol^{-1} when the zero-point energy correction (A basis) is taken into account; moreover, the increasing stabilization of M with respect to m upon going from the La to the Y or Lu model (Tables 1 and S1) does agree with the expected trend.[11] The same energy ordering was indicated by calculations using the A′ basis set, either on water-free models (details are not reported), or on models including the water coligand (Table 1). On the other hand, the use of the larger basis set (B) for the eight-coordinate La models almost zeroed the above energy separation (Table 1), qualitatively producing a more noticeable effect on the energy values than on geometries. In order to put this point in firmer perspective, a set of single point (SP) energy calculations was then performed with the B basis on top of the A-basis optimized $LaDOTA^-$ geometries, not only for the M and m isomers, but also for the higher energy isomers appearing in Table 1, as well as for some of the transition state geometries, to be considered below. For the M and m isomers the SP energy separation (0.19 kcal mol^{-1}) was found to grossly agree with that from the full RHF/B optimizations (0.01 kcal mol^{-1}), suggesting that the differences in SP values so obtained may be considered as reliable estimates of those to be expected from full optimizations at the RHF/B level. Such RHF/B//RHF/A ΔEs for the other systems (reported in footnote *e* of Table S1) generally were 1–2 kcal mol^{-1} smaller than the RHF/A ΔEs. No changes were found in the overall energy ordering from that of the RHF/A picture, which therefore should be referred to with some confidence, the difficult case of the two main isomers being apparently due to their proximity in energy. It should also be recalled that the m/M isomer ratio is known to be solvent-dependent to some extent,[12] according to a delicate balance that these calculations

cannot reproduce. As a distinct quantity, the dissociation energy of $LaDOTA(H_2O)^-$ into $LaDOTA^-$ and H_2O was estimated as the difference of the ZPE-corrected energies of the three optimized models (A′ basis), and was found to amount to 19.7 kcal mol^{-1}.

Geometries of transition states and interconversion mechanisms of the DOTA systems

The investigation on the geometries of transition states (TS) was stimulated in part by the hypothesis, suggested by preliminary molecular mechanics and semiempirical calculations, that in the absence of extensive elongation of metal–donor atom bonds the geometry interconversions should be substantially synchronous, as far as the motion of the pendant arms is concerned, in order to avoid high energy arrangements. It is appropriate to recall that effects due to the solvent are not considered here; it may be tentatively assumed that they do not play a decisive role with these tightly bound chelates. Interactions with the bulk solvent in systems of this type have been modelled *via* MD calculations.[13,17,18] TS geometries were investigated for interconversion pathways joining appropriate enantiomers of the M and m types for DOTA models formed with the La^{3+} or, in part, Y^{3+} cations. Since preliminary results for Lu^{3+} systems were comparable with those for the Y^{3+} ones the Lu^{3+} calculations were discontinued. With reference to Fig. 1 and to the accompanying details for isomer notation, it should be clear that a path connecting the M_1 and m_1 (or, equivalently, the M_2 and m_2) isomers should essentially imply the change of chirality of the carboxylate arms, leaving that of the macrocycle backbone chains unchanged. The $M_1 \leftrightarrows m_2$ (or the $M_2 \leftrightarrows m_1$) isomerization involves the change of chirality of the backbone chains, whereas the $M_1 \leftrightarrows M_2$ and $m_1 \leftrightarrows m_2$ enantiomerizations (these two processes are not equivalent) imply a complete chirality change, for both arms and chains. TS geometries were sought by the synchronous transit-guided quasi-Newton procedure (STQN)[25,34] between pairs of the above geometries, providing in some cases a guess for the TS geometry, if convergence difficulties were encountered or in order to explore regions of interest in parameter space. In spite of the relative complexity of the systems and of the medium-level of the models, it was expected that at least semiquantitative information would be obtained, considering in particular that these processes involve conformational rearrangements, presumably with no change in connectivity. Although the STQN calculational procedure does not perform a systematic scan of the energy hypersurface, it was generally found to monitor ample domains of sensible parameter values. Therefore, although the existence of additional low-energy transition states with respect to those here reported cannot be excluded, the present ones should form a good representative set for the most direct paths between the basic conformations.

Information about the TS geometries and their energies is reported in Table 2 (Y systems in Table S2) and several geometries are schematically shown in Fig. 3. Data in the first two rows of the table and the representations of Fig. 3(a, b) refer to TS geometries pertaining to C_4 symmetry paths. Although such idealized paths are likely to yield high TS energies (but see below for the $M_1 \leftrightarrows m_1$ isomerization) they may be considered for comparison purposes and the associated energies should represent upper limits to acceptable values. For both metal systems, the $M_1 \leftrightarrows m_1$ isomerization, corresponding to the intuitively simplest process (carboxylate arms chirality change), exhibits by far a lower TS energy than the other C_4 process. Two aspects should be noted in this connection. First, several attempts to break the fourfold symmetry of the $M_1 \leftrightarrows m_1$ path failed, substantially yielding in all cases the C_4 TS model and its energy. This should indicate that the carboxylate arm chirality inversion along a "direct" and relatively low-energy path of the present type is attained through a synchronous mechanism and that the corresponding TS energy may be regarded on the same grounds as those of the other TS states, to be considered below, reached in the absence of symmetry constraints. Second, a characteristic feature of the $M_1 \leftrightarrows m_1$ TS geometries, both for La and Y systems, consists of an appreciable elongation of the metal–nitrogen bonds (this is evident, in particular, if compared to the average values of such distances found for other saddle points), probably imposed by the "abnormal" value of the T_{NO} angle. Such elongation seems to be determined by requirements of the ligand cage and is scarcely sensitive to specific metal atom dimensions (the distances of the metal atom from the planes through the oxygens and through the nitrogens are closely similar for La and Y, at variance with the situation found for the limiting M and m geometries, Table S4); it is therefore comparatively larger for the smaller cation. This may rationalize the increase in the barrier height for this path, which is found on

Table 2 Geometrical properties and energies of transition states for conformational rearrangements of $LaDOTA^-$ [a]

Interconversion type[b]	No.	D_N[c]	D_O[c]	T_{NO}[c]	T_{NN}[c]	ΔE[d]
$M_1 \leftrightarrows m_1$[e]	1[f]	3.062	2.398	−16.1	−72.1	21.3
$M_1 \leftrightarrows m_2$ ($M_1 \leftrightarrows M_2$)[g]	2[h]	2.848	2.450	46.8	0.7	61.9
$M_1 \leftrightarrows m_2$[i]	3	2.901, 2.892	2.437, 2.447	43.6, 46.4	5.00, −68.8	15.6
		2.895, 2.842	2.437, 2.443	43.7, 35.1	−60.1, −58.9	
	4	2.856, 2.914	2.452, 2.434	42.1, 49.7	2.0, −64.7	17.8
		2.853, 2.945	2.425, 2.445	34.1, 38.0	−59.9, 57.9	
	5	2.854, 2.846	2.418, 2.477	34.6, 45.0	2.7, 59.5	16.6
		2.936, 2.894	2.455, 2.425	42.9, 38.4	67.2, −55.4	
	6	2.909, 2.967	2.424, 2.456	36.1, 52.3	−3.1, 61.2	17.1
		2.823, 2.888	2.457, 2.435	32.0, 33.6	68.0, 57.4	
$M_1 \leftrightarrows M_2$	7[j]	3.091, 3.246	2.391, 2.388	−35.5, −12.7	−76.4, 71.1	19.5
		2.988, 2.950	2.441, 2.397	32.4, 34.4	49.5, 64.0	

[a] RHF calculations and A basis used throughout. Data in the upper part of the table (rows above the gap) refer to processes performed under C_4 symmetry restrictions; data in the lower part are for processes with no symmetry constraints. [b] See text and Fig. 1 for notation of isomers. [c] Meaning of symbols and conventions for presenting geometrical data are specified in footnote ‡ in the text. [d] Energy differences (kcal mol^{-1}) from the energy of the M isomer are reported. [e] Symmetry-unrestricted paths give results indistinguishable from the C_4 $M_1 \leftrightarrows m_1$ pathway. [f] Geometry shown in Fig. 3(a). [g] Saddle point found also for the $M_1 \leftrightarrows M_2$ path (see note § in the text). [h] Geometry shown in Fig. 3(b). [i] TSs of symmetry-unrestricted pathway of $LaDOTA^-$ system, connecting the M_1 and m_2 isomers (sequentially, from TS no. 3 to no. 6; the intermediate relative minima are, in the order, conformers p, n and q reported in Table 1). The TS geometries are shown in Fig. 3(c–f). [j] Saddle point joining the $M_1 \leftrightarrows m_2$ path of TSs 3–6 and its mirror symmetric path; allows $M_1 \leftrightarrows M_2$ (and $m_1 \leftrightarrows m_2$) interconversion, see text.

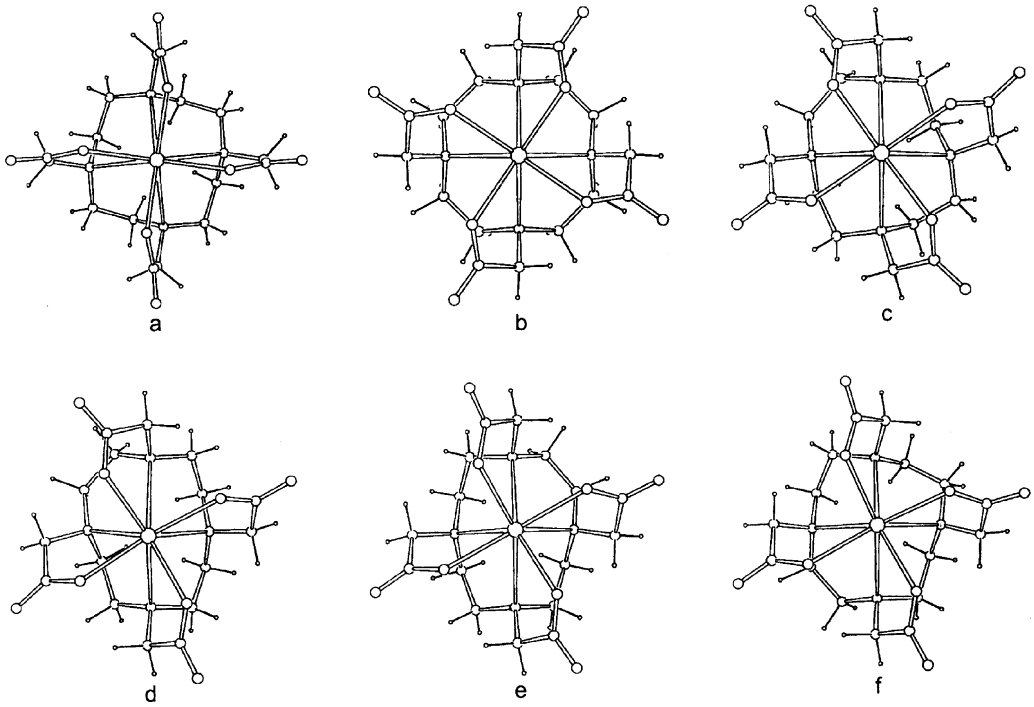

Fig. 3 Geometries of transition states (TS) for $LaDOTA^-$ geometry interconversions (see text and Table 2 for details). (a) TS of the $M_1 \leftrightarrows m_1$ process, no. 1 in Table 2, having effective C_4 symmetry. (b) TS of idealized C_4 symmetry path, for the $M_1 \leftrightarrows m_2$ interconversion, no. 2 in Table 2. (c) First TS, no. 3 in Table 2, along the $M_1 \rightarrow m_2$ path. (d) Second TS (no. 4) of the $M_1 \rightarrow m_2$ path. (e) Third TS (no. 5) of the $M_1 \rightarrow m_2$ path. (f) Fourth TS (no. 6) of the $M_1 \rightarrow m_2$ path.

going from the La to the Y model (Table S2; consistent results, not reported, were obtained for Lu and Sc models). The $M_1 \leftrightarrows m_2$ (isomerization by macrocycle chain chirality changes) and $M_1 \leftrightarrows M_2$ (enantiomerization) processes were found to possess a common TS for the La model in C_4 symmetry [no. 2 in Table 2, Fig. 3(b)].§ Computational difficulties were encountered in the geometry optimizations for the $M_1 \leftrightarrows M_2$ path with the Y^{3+} cation and that process was not further investigated. The energy of this symmetry-imposed TS is evidently too high for such a path to be of practical significance.

Information on the nature of the transition states that should actually be encountered (presumably in addition to the above C_4 $M_1 \leftrightarrows m_1$ TS) in the isomerization or enantiomerization processes is provided by the results obtained in the search of pathways without symmetry restrictions; these are reported in the lower parts of Tables 2 and S2. It should be considered that additional TS geometries, mirror images of those listed, are implied: for example, TS geometries for the $M_2 \leftrightarrows m_1$ interconversion that have T_{NO} and T_{NN} values with signs changed with respect to those of the corresponding step reported for the $M_1 \leftrightarrows m_2$ process. Although each TS in the table is associated with a specific interconversion process, the assignment may not be unique nor unambiguous, due to possible concatenation of pathways and to the existence of branching paths, as may appear from the following discussion.

The results of these investigations on the Y systems (Table S2) parallel those obtained for the La ones. Overall, the TS energies increase with decreasing metal ion size, similarly to what has been noted above for the $M_1 \leftrightarrows m_1$ symmetry-constrained path. An analogous trend has been found experimentally and has been attributed to increased rigidity of the coordination cage following the increase in the metal ion's charge/radius ratio.[7]

Restricting consideration to the La model geometries, it was possible to map with reasonable accuracy the $M_1 \leftrightarrows m_2$ pathway, along which TSs no. 3–6 were detected. The limiting M_1 and m_2 conformations of such a path may be read from Table 1 (m_2 has opposite T_{NO} and T_{NN} signs with respect to those of the m_1 geometry, listed in Table 1). The geometries of the above four TSs are schematically shown in Fig. 3(c–f). The chirality of the pendant arms is preserved along this path, which provides additional support for the original assumption that intramolecular crowding should prevent asynchronous motion of the pendant arms along low-energy pathways. On the other hand, the T_{NO} values, although sign-consistent, are rather spread as a consequence of the pronounced disarray of the macrocycle chains: for all of these TSs one of the T_{NN} values is found to be close to zero and the other three (substantially *gauche*) torsion angles have either alternating signs or have all the same sign. Similar arrangements have been identified previously for cyclododecane's TSs;[39,40] details are given in the footnotes of Table S2. Also the relative uniformity in the present TS no. 3–6 energies recalls the trend noted for the transition states of medium and large size cycloalkanes, and previous comments[39b] may apply also to the present systems in spite of the numerous constraints imposed on the macrocycle ring. The minimum energy conformations denoted "p", "n" and "q" above (Table 1 and Fig. 2) are respectively intermediate between the TS pairs 3–4, 4–5 and 5–6. The $M_1 \leftrightarrows m_2$ (or $M_2 \leftrightarrows m_1$) path now under discussion, which involves macrocycle ring chirality inversion, provides an energetically convenient alternative for isomerization with respect to the one-step $M_1 \leftrightarrows m_1$ process involving TS no. 1, although different isomer combinations, of the M and m type, are involved in the two processes. Attempts to identify a distinct path for the $M_1 \leftrightarrows M_2$ enantiomerization generally produced TS geometries already assigned to the $M_1 \leftrightarrows m_2$ or

§ We are indebted to a reviewer for calling to our attention that this result for the symmetry-constrained paths likely means that such a saddle point pertains to the $M_1 \leftrightarrows m_2$ interconversion (indeed, the T_{NO} value is close to those of the limiting geometries), whereas the $M_1 \leftrightarrows M_2$ interconversion may take place in two steps, $M_1 \leftrightarrows m_2$ and $m_2 \leftrightarrows M_2$, similarly to what is suggested here for the symmetry-unconstrained processes.

$M_2 \leftrightarrows m_1$ pathway, suggesting that the enantiomerization may share some step sequences with the isomerization process. Saddle points were then sought, which would join points of the $M_1 \leftrightarrows m_2$ path with those of its $M_2 \leftrightarrows m_1$ mirror, in order to track the conditions for the change in chirality of the carboxylate arms, which is required, together with the other changes, for the enantiomerization to occur. Such a search yielded TS no. 7 in Table 2, which is the only TS found for these systems having (i) inconsistent T_{NO} signs and (ii) a macrocycle geometry corresponding to that of a cyclododecane *minimum* energy conformation, rather than to that of a transition state (the existence of one imaginary vibrational frequency for the stationary state no. 7 was checked by an independent frequency calculation). In connection with point (i) and with the above discussion of the TS no. 1 geometrical features, it is not surprising that the La–N distances of no. 7 are longer than those of all the $M_1 \leftrightarrows m_2$ path saddle points, their mean (3.07 Å) being even slightly larger than the value for the symmetric TS no. 1. The relative energy of TS no. 7, moderately higher than those of TSs encountered along the $M_1 \leftrightarrows m_2$ path, is in keeping with the experimental observation of a higher activation energy for enantiomerization than for the isomerization process.[7] An alternative pathway for enantiomerization, according to these calculations, might consist of the sequence of two isomerization processes; for example, it could be attained by the $M_1 \leftrightarrows m_2$ interconversion followed by the $m_2 \leftrightarrows M_2$ one, or *vice versa*, from M_2 through m_1 to M_1 (the pathway of TS no. 1 or its mirror symmetric then representing the highest energy step). A similar sequence of pathways, in different order, such as $m_1 \leftrightarrows M_1$ followed by $M_1 \leftrightarrows m_2$, would exchange the m_1 and m_2 geometries at a comparable energy cost to that of the $M_1 \leftrightarrows M_2$ interconversion. Actually, in spite of prolonged efforts, no new TS was detected for a path directly connecting the m_1 and m_2 enantiomers; rather, the above TS no. 5 was found, suggesting that this interconversion occurs *via* combinations of the pathways already described.

As a final comment on these processes, the energies of the transition states in Table 2 (excluding that of TS no. 2) are in the range of the experimental values for systems of this category,[7,41] although detailed comparisons are prevented by mismatch of metal atom type and by the limitations of the present models, pointed out above. The values calculated for the $M_1 \leftrightarrows m_1$ process undergone by the La and Y systems bracket that obtained at a moderately higher level of computation for the Gd complex (with coordinated water molecule).[16] Although some favourable amount of error cancellations in the present case cannot be excluded, the results are encouraging. It should also be recalled that only energy differences are considered here and, mostly, comparisons among these are of interest.

Geometries and transition states of DOTA-like models

The investigation on the DOTA-like complexes formed by the L^{2-} ligand with the La^{3+} and Y^{3+} cations was less extensive than that on the DOTA models, due to the higher complexity of the former systems. In particular, only one TS was sought for each of the geometry interconversion paths, in order to gain some knowledge of its geometry and energy, but detailed studies of the pathways could not be done. On the other hand, simplifying assumptions, such as the substitution of a hydrogen atom for the heterocycle methyl group were avoided, in order to model as accurately as possible the basicity of the methylimidazole nitrogen atom, within the limitations of the basis set being used. The calculations were mostly at the RHF/A level, a few SP energies being computed with basis B. No experimentally determined structures formed by metal trications with this ligand are available for comparisons. Molecular mechanics and semiempirical calculations, followed by the *ab initio* optimizations, yielded the two fundamental geometries, with dihedral angle values close to those of the DOTA complexes. This allows the extension of the assignment of the M and m symbols to the DOTA-like models. The two main isomers are shown in Fig. 4; geometrical parameters and energy values for the La systems are given in Table 3 and full data in Table S3. The m isomer is calculated to lie at lower energy than the M one, for both metal cations, differently from what was found for the DOTA models, but in agreement with the experimental results for some L^{2-} lanthanide derivatives.[22] Also, the partial stabilization of the M *vs.* m form going from the La to the Y models agrees with the experimental trend, verified for the La and Lu compounds.[22] The D_N and D_O values (see Fig. 4 for notation) for the L^{2-} models are moderately smaller than those calculated for the corresponding (in the nature of metal and isomer type) DOTA models (Tables 1 and 3). Going from the LaL^+ to the YL^+ systems the D_{Nim} values decrease considerably (*ca.* 0.20 Å for each isomer) and the D_N and D_O values decrease slightly less (both by *ca.* 0.16 Å). For the DOTA models the largest decrease, 0.18 Å, is in the D_O values, pertaining to the charged donors, and the D_N values decrease by 0.14 Å. Still going from LaL^+ to YL^+, the metal cation shifts toward the plane through the macrocycle nitrogens, by 0.21 Å, and away from the best plane through the carboxylate oxygens and the imidazole nitrogens, by 0.14 Å, such shifts being both slightly larger than those verified for the DOTA models.

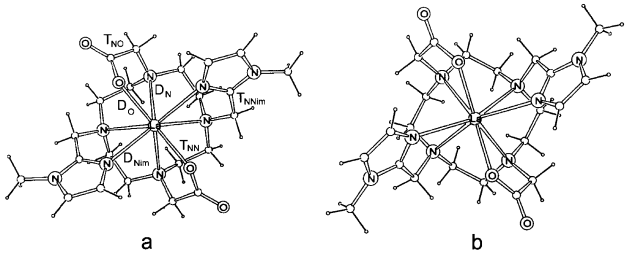

Fig. 4 (a) Geometry of the optimized LaL^+ M_1 isomer, formed by the DOTA-like L^{2-} ligand. The meaning of the D_N, D_O, T_{NO} and T_{NN} symbols is unchanged from that of Fig. 2(a). Parameters specific for the DOTA-like models are: D_{Nim}, for metal–methylimidazole nitrogen distances, and T_{NNim}, for the N–C–C–N_{im} torsion angles of the methylimidazole-bearing arms. (b) Geometry of the optimized LaL^+ m_1 isomer.

In Table 3 data are listed for three additional conformers of LaL^+, which were studied to determine how closely their energies approach that of the most stable isomer, for the same reasons that prompted the investigations on the n, p and q DOTA models. Their geometries are shown in Fig. 5(a–c). Two of these, denoted n and q, possess the same macrocycle conformation as the similarly labelled DOTA isomers, whereas the third one (r), having higher energy, is of a different type ([2343] conformation). Although the n and q LaL^+ isomers are closer in energy to m than are the corresponding DOTA isomers to their M counterpart, no signals were detected in the LaL^+ NMR spectra that might be attributed to those isomers.[22] ZPE-corrected energies at the RHF/A level and SP RHF/B//RHF/A energy values (Table S3) are not such as to modify the energy ordering of Table 3. Examining the geometrical parameters of the five LaL^+ isomers in the upper part of Table 3, the values of the T_{NO} and T_{NNim} torsion angles of the arms are seen to spread increasingly as the isomer energy increases. This does not involve important lengthening of metal–donor atom distances and is presumably allowed by the lower overall charge borne by the dangling groups and/or by its different distribution with respect to the DOTA systems. The greater versatility of the L^{2-} systems' pendant arms is clearly revealed by the TS geometries, discussed next.

Table 3 Minimum energy and transition state conformations of the LaL^+ DOTA-like model[a]

Geometry or interconversion type[b]	D_N[c]	D_O[c]	D_{Nim}[d]	T_{NO}[c]	T_{NNim}[d]	T_{NN}[c]	ΔE[e]
m[f]	2.838, 2.828	2.384	2.651	−32.1	−25.2	−62.5, −61.1	0
M[g]	2.814, 2.856	2.386	2.643	42.5	30.6	−58.1, −64.8	2.5
n	2.839, 2.793	2.399	2.636	46.2	29.3	58.0, −55.1	4.5
q	2.926, 2.775	2.379	2.649	47.2	24.6	54.3, 60.7	4.2
	2.849, 2.781	2.409	2.637	22.6	29.8	−59.3, 60.1	
r	2.918, 2.782	2.364	2.665	49.0	16.5	56.6, 54.9	9.4
	2.844, 2.859	2.401	2.631	52.2	8.3	−56.7, −67.8	
$m_2 \leftrightarrows M_2$	2.988, 2.924	2.357	2.623	−46.6	17.0	67.1, 72.8	15.1
	2.938, 2.859	2.361	2.647	39.6	30.4	65.4, 67.8	
$m_2 \leftrightarrows M_1$	2.823, 2.810	2.416	2.635	60.9	27.5	5.8, 60.0	13.6
	2.786, 2.842	2.390	2.632	46.7	22.9	63.6, −56.6	
$M_1 \leftrightarrows M_2$	3.026, 2.829	2.381	2.632	54.6	−29.8	−4.4, −54.6	27.8
	2.832, 2.858	2.372	2.638	44.0	−34.7	−65.8, 52.5	
$M_1 \leftrightarrows M_2$ (C_2)	2.879, 2.831	2.380	2.647	40.7	−27.5	−3.7, −50.7	36.1

[a] RHF calculations and A basis used. Data in the upper part of the table refer to minimum energy conformations, those in the lower part to transition state geometries. [b] Either C_2 or C_1 symmetry present. [c] Symbols with the same meaning as in Tables 1 and 2. [d] Parameters specific for the DOTA-like models, see Fig. 4(a) for definitions. [e] Energy differences (kcal mol^{-1}) with respect to the m isomer [E(LaL^+, m) = 1618.15302 Hartrees]. [f] Data are for the m_1 isomer, shown in Fig. 4(b). [g] Data for the M_1 isomer, shown in Fig. 4(a).

The saddle point geometry for the $m_2 \leftrightarrows M_2$ interconversion [Table 3 and Fig. 5(d)] differs from that of the DOTA $M_1 \leftrightarrows m_1$ pathway (this is not due to the fact that enantiomeric systems were studied in the two cases) in important respects: (a) symmetry properties (C_2 symmetry would now correspond to the previous C_4) are no longer present, (b) two pendant arms, those bearing the carboxylate groups, have opposite chirality, (c) the energy separation from the m isomer is definitely smaller than the ΔE of the corresponding process for the DOTA model. This is apparently to be ascribed to the substitution of two neutral methylimidazole groups in the ligand for two carboxylates in *trans* positions, which should decrease the electrostatic repulsions between the coordinating pendant arms. Although the Mulliken charges[42] on the imidazole nitrogens are marginally smaller than those on the carboxylate oxygens, their repulsive effects should be diminished by the contributions to the electrostatic potential due to the other atoms in the heterocyclic rings.

The conformation at the saddle point attributed to the $m_2 \leftrightarrows M_1$ pathway in Table 3 may be compared with that of TS no. 5, $M_1 \leftrightarrows m_2$ path, in Table 2 and Fig. 5(e), properly reoriented, may be compared with Fig. 3(e). However, the ΔE for the DOTA-like model is definitely lower than the other one, which may be due again to smaller repulsive effects. Similarly, the symmetrical (C_2) TS for the $M_1 \leftrightarrows M_2$ interconversion, reported in the last row of Table 3, has ΔE almost 50% smaller than that of the DOTA C_4-symmetry TS, no. 2 in Table 2; the barrier height, however, is still too high for the path of the LaL^+ symmetrical saddle point to be practicable. On the other hand, it is dubious that a DOTA system could reach a C_2-symmetry saddle point of the type now under dicussion for the LaL^+ species, which exhibits opposite chirality for pairs of pendant arms.

An extensive search with no symmetry constraints along the path of the same $M_1 \leftrightarrows M_2$ interconversion produced the TS whose parameters are listed in the penultimate row of Table 3.

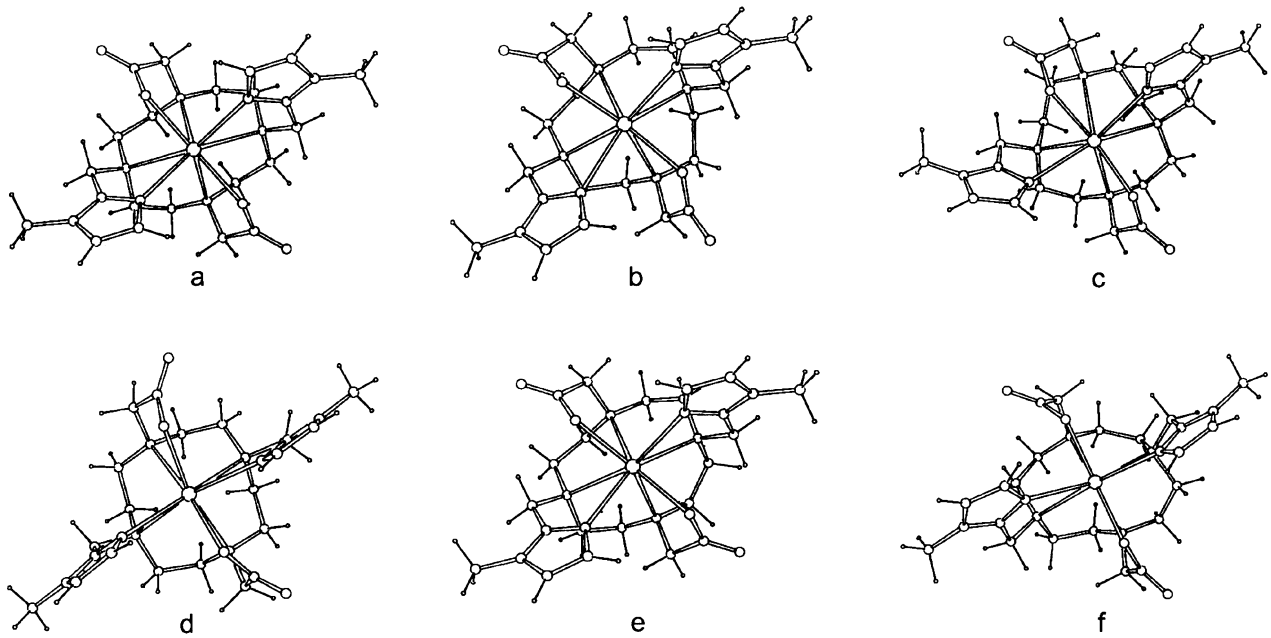

Fig. 5 (a) Schematic representation of the geometry of the n isomer of LaL^+. (b) Geometry of the q LaL^+ isomer. (c) Geometry of the r LaL^+ isomer. (d) TS geometry for the $m_2 \leftrightarrows M_2$ interconversion pathway of LaL^+. (e) TS geometry for the $m_2 \leftrightarrows M_1$ interconversion pathway of LaL^+. (f) TS geometry for the symmetry-unconstrained $M_1 \leftrightarrows M_2$ interconversion pathway of LaL^+.

This has the same macrocycle conformation as the TS of the $m_2 \leftrightarrows M_1$ isomerization pathway, but exhibits opposite chirality for the two types of pendant arms [Fig. 5(f)]. As for the above TS geometry for the $m_2 \leftrightarrows M_2$ interconversion, the present one also was not detected for DOTA systems. It is characterized by a remarkably high energy, for a symmetry-unrestricted process. The relative uniformity in TS ΔE values found for the DOTA models does not hold for the DOTA-like ones, which is likely caused by the lack of even approximate uniformity in the arrangement of their pendant arms. If no other direct pathway, more convenient than the last mentioned, is available for the enantiomerization process of the L^{2-} models, it should be assumed that the enantiomerization takes place through sequences of interconversion, such as $m_2 \leftrightarrows M_1$ followed by $M_1 \leftrightarrows m_1$. Overall, this would imply a barrier *ca*. 10% higher than that for the simple isomerization, occurring through the single $m_2 \leftrightarrows M_1$ process (or its symmetry related). The lower barrier height, for the simple isomerization process, is in reasonable agreement with the experimental value of $\Delta H^{\ddagger} = 14.7 \pm 0.5$ kcal mol^{-1}, from ^{13}C NMR spectra in D_2O.[22]

Conclusions

This study has provided information on stationary states of the title model complexes, allowing comparisons between isomer geometries, showing effects of changes in metal ion size, and presenting possible transition state geometries for isomer interconversion pathways. Similarities as well as differences between DOTA and L^{2-} systems have emerged. Limitations in the basis set and neglect of the water coligand in the gaseous state models suggest that overall trends, rather than individual results, should be taken into consideration. However, the broad agreement with experimental energy barrier heights and the detection of strong similarities in both minimum energy and well-established transition state conformations of the cyclic hydrocarbon matching the present macrocycle in size add confidence in the significance of the results. It is hoped that the possibility to use in the future larger and better basis sets for more extensive investigations will allow to check and extend these results.

Acknowledgement

Financial support by the Italian Ministero dell'Università e della Ricerca Scientifica e Tecnologica is gratefully acknowledged.

References

1 J. F. Desreux, *Inorg. Chem.*, 1980, **19**, 1319.
2 M. R. Spirlet, J. Rebizant, J. F. Desreux and M. F. Loncin, *Inorg. Chem.*, 1984, **23**, 359.
3 S. Aime, M. Botta and G. Ermondi, *Inorg. Chem.*, 1992, **31**, 4291.
4 S. Aime, P. L. Anelli, M. Botta, F. Fedeli, M. Grandi, P. Paoli and F. Uggeri, *Inorg. Chem.*, 1992, **31**, 2422.
5 C. A. Chang, L. C. Francesconi, M. F. Malley, K. Kumar, J. Z. Gougoutas, M. T. Tweedle, D. W. Lee and L. J. Wilson, *Inorg. Chem.*, 1993, **32**, 3501.
6 D. Parker, K. Pulukkody, F. C. Smith, A. Batsanov and J. A. K. Howard, *J. Chem. Soc., Dalton Trans.*, 1994, 689.
7 S. Aime, A. Barge, M. Botta, M. Fasano, J. D. Ayala and G. Bombieri, *Inorg. Chim. Acta*, 1996, **246**, 423.
8 S. Aime, A. Barge, F. Benetollo, G. Bombieri, M. Botta and F. Uggeri, *Inorg. Chem.*, 1997, **36**, 4287.
9 H. Maumela, R. D. Hancock, L. Carlton, J. H. Reibenspies and K. P. Wainwright, *J. Am. Chem. Soc.*, 1995, **117**, 6698.
10 J. A. K. Howard, A. M. Kenwright, J. M. Moloney, D. Parker, M. Port, M. Navet, O. Rousseau and M. Woods, *Chem. Commun.*, 1998, 1381.
11 S. Aime, M. Botta, M. Fasano, M. P. M. Marques, C. F. G. C. Geraldes, D. Pubanz and A. E. Merbach, *Inorg. Chem.*, 1997, **36**, 2059.
12 S. Aime, A. Barge, J. I. Bruce, M. Botta, J. A. K. Howard, J. M. Moloney, D. Parker, A. S. de Sousa and M. Woods, *J. Am. Chem. Soc.*, 1999, **121**, 5762.
13 R. Fossheim and S. G. Dahl, *Acta Chem. Scand.*, 1990, **44**, 698.
14 D. E. Reichert, R. D. Hancock and M. J. Welch, *Inorg. Chem.*, 1996, **35**, 7013.
15 C. Lecomte, V. Dahaoui-Gindrey, H. Chollet, C. Gros, A. K. Mishra, F. Barbette, P. Pullumbi and R. Guilard, *Inorg. Chem.*, 1997, **36**, 3827.
16 U. Cosentino, G. Moro, D. Pitea, A. Villa, P. C. Fantucci, A. Maiocchi and F. Uggeri, *J. Phys. Chem. A*, 1998, **102**, 4606.
17 A. Varnek, G. Wipff, A. Bilyk and J. M. Harrowfield, *J. Chem. Soc., Dalton Trans.*, 1999, 4155.
18 S. Durand, J. P. Dognon, P. Guilbaud, C. Rabbe and G. Wippf, *J. Chem. Soc., Perkin 2*, 2000, 705.
19 A. Villa, U. Cosentino, D. Pitea, G. Moro and A. Maiocchi, *J. Phys. Chem. A*, 2000, **104**, 3421.
20 (*a*) E. J. Corey and J. C. Bailar, *J. Am. Chem. Soc.*, 1959, **81**, 2620; (*b*) J. K. Beattie, *Acc. Chem. Res.*, 1971, **4**, 253.
21 M. Di Vaira, F. Mani and P. Stoppioni, *J. Chem. Soc., Dalton Trans.*, 1998, 1879.
22 F. Mani, R. Morassi, P. Stoppioni and A. Vacca, *J. Chem. Soc., Dalton Trans.*, 2001, 2116.
23 PCMODEL release 7.0 for Windows, Serena Software, Bloomington, IN, USA, 1998.
24 HyperChem release 5.0 for Windows, Hypercube Inc., Waterloo, Ontario, Canada, 1996.
25 M. J. Frisch, G. W. Trucks, H. B. Schlegel, G. E. Scuseria, M. A. Robb, J. R. Cheeseman, V. G. Zakrzewski, J. A. Montgomery, Jr., R. E. Stratmann, J. C. Burant, S. Dapprich, J. M. Millam, A. D. Daniels, K. N. Kudin, M. C. Strain, O. Farkas, J. Tomasi, V. Barone, M. Cossi, R. Cammi, B. Mennucci, C. Pomelli, C. Adamo, S. Clifford, J. Ochterski, G. A. Petersson, P. Y. Ayala, Q. Cui, K. Morokuma, D. K. Malick, A. D. Rabuck, K. Raghavachari, J. B. Foresman, J. Cioslowski, J. V. Ortiz, A. G. Baboul, B. B. Stefanov, G. Liu, A. Liashenko, P. Piskorz, I. Komaromi, R. Gomperts, R. L. Martin, D. J. Fox, T. Keith, M. A. Al-Laham, C. Y. Peng, A. Nanayakkara, C. Gonzalez, M. Challacombe, P. M. W. Gill, B. Johnson, W. Chen, M. W. Wong, J. L. Andres, C. Gonzalez, M. Head-Gordon, E. S. Replogle and J. A. Pople, Gaussian 98, Rev. A.7, Gaussian, Inc., Pittsburgh, PA, USA, 1998.
26 A. D. Becke, *J. Chem. Phys.*, 1993, **98**, 5648.
27 C. Lee, W. Yang and R. G. Parr, *Phys. Rev. B*, 1998, **37**, 785.
28 P. J. Hay and W. R. Wadt, *J. Chem. Phys.*, 1985, **82**, 270.
29 R. Ditchfield, W. J. Hehre and J. A. Pople, *J. Chem. Phys.*, 1971, **54**, 724.
30 A. D. McLean and G. S. Chandler, *J. Chem. Phys.*, 1980, **72**, 5639.
31 R. Krishnan, J. S. Binkley, R. Seeger and J. A. Pople, *J. Chem. Phys.*, 1980, **72**, 650.
32 M. Dolg, H. Stoll, A. Savin and H. Preuss, *Theor. Chim. Acta*, 1989, **75**, 173.
33 A. Bergner, M. Dolg, W. Küchle, H. Stoll and H. Preuss, *Mol. Phys.*, 1993, **80**, 1431.
34 C. Peng, P. Y. Ayala, H. B. Schlegel and M. J. Frisch, *J. Comput. Chem.*, 1995, **16**, 49.
35 M. Nardelli, *J. Appl. Crystallogr.*, 1995, **28**, 659.
36 G Schaftenaar and J. H. Noordik, *J. Comput. Aided Mol. Des.*, 2000, **14**, 123.
37 (*a*) C. K. Johnson, ORTEP, Report ORNL-5138, Oak Ridge National Laboratory, Oak Ridge, TN, USA, 1976; (*b*) L. J. Farrugia, *J. Appl. Crystallogr.*, 1997, **30**, 565.
38 R. D. Shannon and C. T. Prewitt, *Acta Crystallogr., Sect. B*, 1969, **25**, 925.
39 (*a*) J. Dale, *Acta Chem. Scand.*, 1973, **27**, 1115; (*b*) J. Dale, *Acta Chem. Scand.*, 1973, **27**, 1130.
40 F. A. L. Anet and T. N. Rawdah, *J. Am. Chem. Soc.*, 1978, **100**, 7166.
41 V. Jacques and J. F. Desreux, *Inorg. Chem.*, 1994, **33**, 4048.
42 R. S. Mulliken, *J. Chem. Phys.*, 1955, **23**, 1833.